Journal of Superconductivity: Incorporating Novel Magnetism, Vol. 16, No. 5, October 2003 (© 2003)

Experiments and Model of Intermodulation Distortion in a Rutile Resonator with Y-Ba_2-Cu_3-$O_{7-\delta}$ Endplates

J. Mateu,[1] C. Collado,[2] O. Menéndez,[2] and J. M. O'Callaghan[2]

Received September 30, 2002

We have derived general equations to calculate intermodulation distortion in resonators with high temperature superconducting (HTS) films which are not restricted to a specific resonator shape and may be used whenever the fields in a resonator generate currents on the surface of one or more HTS films. These equations are applied to rutile-loaded cavities with one or two $10 \times 10\,\text{mm}^2$ Y-Ba_2-Cu_3-$O_{7-\delta}$ endplates and are used to extract parameters characterizing the nonlinearities of these films from intermodulation measurements. Even though the films have similar small-signal performance, we have found large variation in the strength of their nonlinearities.

KEY WORDS: nonlinear measurements; dielectric cavity; intermodulation measurements; superconductors.

1. INTRODUCTION

High Temperature Superconducting (HTS) thin films are being used in narrowband microwave filters due to their low losses and small volume. The use of HTS materials in this application might be limited by their nonlinearities, which give rise to intermodulation distortion (IMD) and other undesired effects [1]. Although most of the experimental work on HTS intermodulation has been done on planar patterned devices [2–4], this type of characterization might not be representative of the properties of the whole HTS film because the nonlinear properties of the test devices are dominated by the high current densities at the edges of the pattern, where the properties of the film may be affected by the etching process. In this work we describe a technique that might contribute to overcome these difficulties, which is based on the use of a rutile resonator to make a small-area characterization of the intermodulation properties of unpatterned HTS films.

[1]CTTC-Centre Tecnològic de Telecomunicacions de Catalunya, Edifici NEXUS, C/Gran Capità 2–4, 08034 Barcelona, Catalunya, Spain.

[2]Universitat Politecnica de Catalunya, Campus Nord UPC-D3, C/Jordi Girona 1, 08034 Barcelona, Spain.

2. A GENERAL FORMULATION FOR HTS NONLINEARITIES

We assume that, at high currents, the electric field at the surface of the superconductor is the sum of a linear contribution due to the surface impedance of the film, plus an additional electric field $\overrightarrow{e_{\text{NL}}}$ caused by the nonlinearities [5, 6] which can be expressed as

$$\overrightarrow{e_{\text{NL}}}(j_s) = a_{\text{NL}}(j_s)\vec{j}_s + \frac{\partial}{\partial t}\left[b_{\text{NL}}(j_s)\vec{j}_s\right], \qquad (1)$$

where $\vec{j}_s$ is the surface current density, $a_{\text{NL}}(j_s)$ represents the nonlinear resistive term, and $b_{\text{NL}}(j_s)$ the nonlinear reactive term. Both terms depend on the magnitude of the surface current j_s and have to be zero for $j_s = 0$ to make $\overrightarrow{e_{\text{NL}}}$ vanish at arbitrarily small currents.

An alternative form of describing the nonlinearities in the HTS consists in quantifying the change in surface impedance as a function of the surface current density (or magnetic field), i.e., in frequency domain we would have $\vec{E}_{\text{NL}} = \Delta R_s(J_s)\vec{J}_s + j\Delta X_s(J_s)\vec{J}_s$ [3], where $\Delta R_s(J_s) + j\Delta X_s(J_s)$ is the variation in surface impedance with respect the small signal value. While finding the equivalence between this formulation and the one in Eq. (1) is straightforward (see Fig.

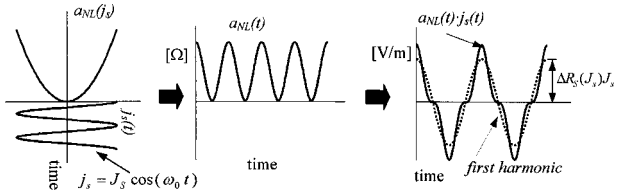

Fig. 1. Comparison between $a_{\mathrm{NL}}(t)\, j_{\mathrm{s}}(t)$ in time domain (solid line in rightmost graph) and the deviation of the surface resistance from its small-signal value (ΔR_{s} proportional to the amplitude of the sinusoid drawn with dotted line in the rightmost graph).

1), we prefer that in Eq. (1) since it gives all the details of the time-domain function, whereas ΔR_{s}, ΔX_{s} only refer to its first harmonic.

Another existing formulation for HTS nonlinearities that can be related to that in Eq. (1) is the one described in [7, 8], according to which the penetration depth depends on the current density. This formulation has been extensively used to justify the generation of IMD in HTS films, and our previous work [9], shows how it can be related to the nonlinear reactive term $b_{\mathrm{NL}}(j_{\mathrm{s}})$ in Eq. (1). Equation (1) is thus a very general mathematical description of HTS nonlinearities that can be particularized for various models and should account for the generation of both harmonics and intemodulation products.

With little loss in generality, in this work we assume that $a_{\mathrm{NL}}, (j_{\mathrm{s}}), b_{\mathrm{NL}}, (j_{\mathrm{s}})$ can be expressed as $a_{\mathrm{NL}}(j_{\mathrm{s}}) = \Delta R_\alpha |j_{\mathrm{s}}|$, $b_{\mathrm{NL}}(j_{\mathrm{s}}) = \Delta L_\alpha |j_{\mathrm{s}}|^\alpha$, where α, $\Delta R_\alpha, \Delta L_\alpha$ are parameters that characterize the strength of the nonlinearity in the HTS. Equation (1) will then read

$$\overrightarrow{e_{\mathrm{NL}}} = \Delta R_\alpha |j_{\mathrm{s}}|^\alpha \vec{j}_{\mathrm{s}} + \Delta L_\alpha \frac{d}{dt}\left(|j_{\mathrm{s}}|^\alpha \vec{j}_{\mathrm{s}}\right). \tag{2}$$

3. INTERMODULATION IN HTS RESONATORS

In this section, we will derive general equations for the power of the third-order intermodulation products coupled out of a resonator due to nonlinearities in the HTS. The analysis applies to any resonator where the field configuration of the resonant mode is such that it generates currents on the surface of an HTS material. The dielectric-loaded cavity resonators used for R_{s} measurement of HTS films are an obvious example, but the analysis could also be applied to a disk resonator or to planar, patterned HTS resonators.

3.1. Electric Field due to HTS Nonlinearities

In any resonator the current at the surface of the HTS film can be written as

$$\vec{j}_{\mathrm{s}}(\vec{r}, t) = A(t)\, f(\vec{r})\hat{u}(\vec{r}), \tag{3}$$

were $\hat{u}(\vec{r})$ is a unit vector, $f(\vec{r})\hat{u}(\vec{r})$ describes the spatial dependence of the current density, and $A(t)$ its time dependence. For the case of an intermodulation experiment $A(t)$ will consist of the sum of two sinusoidal signals with amplitudes j_1 and j_2:

$$A(t) = j_1 \cos\omega_1 t + j_2 \cos\omega_2 t. \tag{4}$$

Combining Eqs. (2)–(4) we find that the electric field at the surface of the superconductor can be written as

$$\overrightarrow{e_{\mathrm{NL}}}(\vec{r}, t) = \left\{\Delta R_\alpha |A(t)|^\alpha A(t) + \Delta L_\alpha \frac{d}{dt}(|A(t)|^\alpha A(t))\right\} \times |f(\vec{r})|^\alpha f(\vec{r})\hat{u}(\vec{r}). \tag{5}$$

Note that the spatial dependence of $\overrightarrow{e_{\mathrm{NL}}}$ (the term $|f(\vec{r})|^\alpha f(\vec{r})\hat{u}(\vec{r})$ in Eq. (5)) differs from that of the current $\vec{j}_{\mathrm{s}}$. From Eq. (5) we can calculate the electric field at $2\omega_1 - \omega_2$:

$$\vec{E}_{2\omega_1-\omega_2} = [\Delta R_\alpha + j(2\omega_1 - \omega_2)\Delta L_\alpha] 2C_{2\omega_1-\omega_2} |f(\vec{r})|^\alpha \times f(\vec{r})\hat{u}(\vec{r}), \tag{6}$$

where $2C_{2\omega_1-\omega_2}$ is the intermodulation produced by the function $|A(t)|^\alpha A(t)$ at $2\omega_1 - \omega_2$and has the units of $(\mathrm{A/m})^{\alpha+1}$, i.e.

$$C_{2\omega_1-\omega_2} = \lim_{T\to\infty} \frac{1}{T} \int_{-\frac{T}{2}}^{\frac{T}{2}} |A(t)|^\alpha A(t) e^{-j(2\omega_1-\omega_2)t} dt. \tag{7}$$

Figure 2 shows the dependence of the electric field amplitude at $2\omega_1 - \omega_2$ and at $2\omega_2 - \omega_1$ as a function of the surface current amplitude j_1 (i.e., $C_{2\omega_1-\omega_2}$ and $C_{2\omega_2-\omega_1}$ vs. j_1). When $j_1 = j_2$ both $C_{2\omega_1-\omega_2}$ and $C_{2\omega_2-\omega_1}$ are proportional to $j_1^{\alpha+1}$, so a logarithmic plot of $C_{2\omega_1-\omega_2}$ versus j_1 or $C_{2\omega_2-\omega_1}$ versus j_1 has a slope of $\alpha + 1$. When $j_1 \ll j_2$, $C_{2\omega_1-\omega_2} \propto j_1^2 j_2$ and $C_{2\omega_2-\omega_1} \propto j_1 j_2^2$ so, if j_2 is kept constant, the slopes in Fig. 2 are 2:1 and 1:1, respectively, regardless of the value of α. In the opposite regime, when $j_1 \gg j_2$, $C_{2\omega_1-\omega_2} \propto j_1^\alpha j_2^{\alpha-1}$ and $C_{2\omega_2-\omega_1} \propto j_1^{\alpha-1} j_2^\alpha$ so, in a logarithmic scale, the magnitude of the electric field at the intermodulation frequency changes with slopes of α and $\alpha - 1$ with the current amplitude j_1 when j_2 is fixed. The dependence of $C_{2\omega_1-\omega_2}$ and $C_{2\omega_2-\omega_1}$ on j_1 and j_2 described here accounts for the experimental results described in the following sections of this work and for those reported in [10].

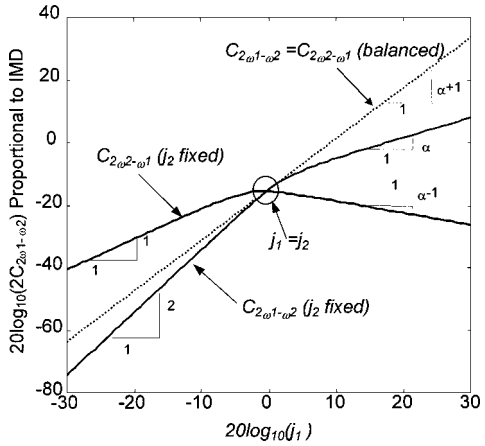

Fig. 2. Dependence of the electric field at the intermodulation frequencies ($2C_{2\omega_1-\omega_2}$ and $2C_{2\omega_2-\omega_1}$) on the amplitude of the surface current j_1.

When the two current amplitudes j_1, j_2 are kept equal to each other, the fraction $C_{2\omega_1-\omega_2}/j_1^{\alpha} j_2$ only depends on the order of the nonlinearity α. Hence, instead of $C_{2\omega_1-\omega_2}(j_1, j_2, \alpha)$, we will use the parameter

$$T_{2\omega_1-\omega_2}(j_1, j_2, \alpha) \equiv \frac{2C_{2\omega_1-\omega_2}(j_1, j_2, \alpha)}{j_1^{\alpha} j_2} \qquad (8)$$

in subsequent equations. Figure 3 shows the dependence of $T_{2\omega_1-\omega_2}$ on α for balanced current amplitudes.

In summary, Eqs. (6)–(8) give a general set of equations relating the IMD electric field at the surface of the superconductor with the amplitude of the surface current density. These equations are not restricted to a particular shape of resonator and should be valid whenever $a_{\mathrm{NL}}(j_s) = \Delta R_{\alpha} |j_s|^{\alpha}$ and $b_{\mathrm{NL}}(j_s) = \Delta L_{\alpha} |j_s|^{\alpha}$.

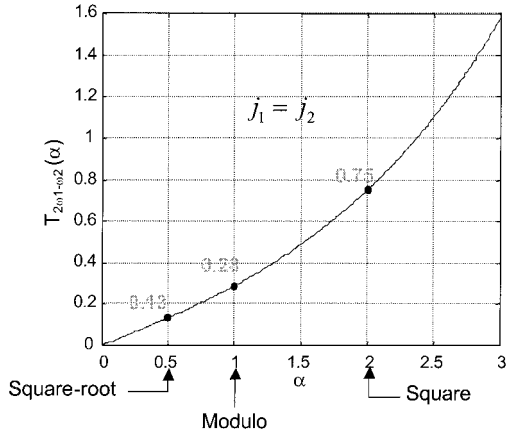

Fig. 3. Dependence of $T_{2\omega_1-\omega_2}$ on the order of the nonlinearity α for balanced current amplitudes. In this case, the amplitude of the electric field at the surface of the HTS at the intermodulation frequency will be proportional to $T_{2\omega_1-\omega_2}(\alpha) j_1^{\alpha+1}$

3.2. Resonant IMD Magnetic Field on the HTS Surface

From the discussion above, we have determined that the IMD electric field on the HTS surface will be of the form

$$\vec{E}_{2\omega_1-\omega_2} = E_{2\omega_1-\omega_2} |f(\vec{r})|^{\alpha} f(\vec{r}) \hat{u}(\vec{r}), \qquad (9)$$

with

$$E_{2\omega_1-\omega_2} = [\Delta R_{\alpha} + j(2\omega_1 - \omega_2)\Delta L_{\alpha}] \times T_{2\omega_1-\omega_2}(j_1, j_2, \alpha) j_1^{\alpha} j_2. \qquad (10)$$

If $\omega_1 \approx \omega_2 \approx 2\omega_1 - \omega_2$ this field will couple to the same mode at which ω_1 and ω_2 resonate and will generate a magnetic field at $2\omega_1 - \omega_2$ whose spatial distribution has to be the same than that of $\vec{j}_s(\vec{r}, t)$ in Eq. (3), i.e.,

$$\vec{H}_{2\omega_1-\omega_2} = H_{2\omega_1-\omega_2} f(\vec{r}) \hat{v}(\vec{r}), \qquad (11)$$

where $\hat{v}(\vec{r})$ is a unit vector on the HTS surface perpendicular to $\hat{\mu}(\vec{r})$. The magnetic field on the HTS at $2\omega_1 - \omega_2$ is thus fully known if we can determine its amplitude $H_{2\omega_1-\omega_2}$. To do that we consider the power generated at the surface of the HTS at $2\omega_1 - \omega_2$:

$$P = \frac{1}{2} \int_S \vec{E}_{2\omega_1-\omega_2} \times \vec{H}^*_{2\omega_1-\omega_2} d\vec{S} \qquad (12)$$

and relate it to the resonator Q. This power will be either dissipated inside the resonator or coupled outwards, so it has to satisfy

$$P = \frac{(2\omega_1 - \omega_2)W}{Q_L}, \qquad (13)$$

where W is the energy stored in the resonator at $2\omega_1 - \omega_2$ and Q_L is the loaded quality factor. If we normalize this energy with respect to the field amplitude $|H_{2\omega_1-\omega_2}|^2$ we get $W_0 = W/|\vec{H}_{2\omega_1-\omega_2}|^2$ and

$$P = \frac{1}{2} \int_S \vec{E}_{2\omega_1-\omega_2} \times \vec{H}^*_{2\omega_1-\omega_2} d\vec{S} = \frac{(2\omega_1 - \omega_2)W_0}{Q_L} H^*_{2\omega_1-\omega_2} H_{2\omega_1-\omega_2}. \qquad (14)$$

Using Eqs. (9)–(11) in Eq. (14) we find $H_{2\omega_1-\omega_2}$:

$$\vec{H}_{2\omega_1-\omega_2}(\vec{r}) = \frac{1}{2}[\Delta R_\alpha + j(2\omega_1-\omega_2)\Delta L_\alpha] \; T_{2\omega_1-\omega_2}(j_1, j_2, \alpha) j_1^\alpha j_2 \frac{Q_L}{(2\omega_1-\omega_2)W_0} \int_S \{|f(\vec{r})|^\alpha f(\vec{r}) f(\vec{r})\, dS\} f(\vec{r})\vec{r}. \quad (15)$$

Note that the term $\frac{1}{2}\int_S |f(\vec{r})|^\alpha f(\vec{r}) f(\vec{r})\, dS$, is a sort of coupling coefficient between the spatial distribution of the electric field on HTS ($|f(\vec{r})|^\alpha f(\vec{r})$) and that of the magnetic field of the resonant mode in the structure ($f(\vec{r})$). If we express this term as Γ_α, Eq. (15) can be written as

$$\vec{H}_{2\omega_1-\omega_2}(\vec{r}) = [\Delta R_\alpha + j(2\omega_1-\omega_2)\Delta L_\alpha] \; T_{2\omega_1-\omega_2}(j_1, j_2, \alpha) j_1^\alpha j_2 \; \Gamma_\alpha \frac{Q_L}{(2\omega_1-\omega_2)W_0} f(\vec{r})\vec{r}. \quad (16)$$

Note that we are assuming that the intermodulation products are only generated by the mixing of the fundamental signals. This means that we are not considering higher order effects that could contribute to $\vec{H}_{2\omega_1-\omega_2}$ like for example the mixing of higher order spurious signals.

3.3. IMD Power Coupled Out of the Resonator

In this section we calculate the power of the intermodulation product coupled out of the structure as a function of the available power of the sources at fundamental frequencies ω_1 and ω_2 (P_{0,ω_1} and P_{0,ω_2}, respectively) and the external coupling factors.

We first analyze the case of a one-port resonator. In this resonator the coupling factor κ is the ratio of the power coupled to the load (P_L) to the power dissipated in the resonator (P_d) [11], so

$$P_L = \kappa P_d = \kappa \frac{(2\omega_1-\omega_2)W}{Q_0} = \kappa \frac{(2\omega_1-\omega_2)W_0}{Q_0}|H_{2\omega_1-\omega_2}|^2, \quad (17)$$

where $|H_{2\omega_1-\omega_2}|$ is given by Eq. (16).

We now have to relate j_1 and j_2 in Eq. (16) with the power available from the sources at ω_1 and ω_2 (P_{0,ω_1} and P_{0,ω_2}). To do this we use the equation that relates dissipated power (P_d) with available power (P_0) in a one-port resonator:

$$P_d = \frac{4P_0\kappa}{(1+\kappa)^2} \quad (18)$$

so, for ω_1

$$\frac{4P_{0,\omega_1}\kappa}{(1+\kappa)^2} = \frac{\omega_1 W_0}{Q_0}|j_1|^2 \quad (19)$$

and similarly for ω_2.

Using Eqs. (16), (18), and (19) for ω_1 and ω_2, and assuming $\omega_1 \approx \omega_2 \approx 2\omega_1-\omega_2 \approx \omega_0$, we get

$$P_L = (4P_{0,\omega_1})^\alpha (4P_{0,\omega_2}) \left(\frac{Q_0}{\omega_0 W_0}\right)^{\alpha+2} \left[\frac{\kappa}{(1+\kappa)^2}\right]^{(\alpha+2)} |[\Delta R_\alpha + j(2\omega_1-\omega_2)\Delta L_\alpha] T_{2\omega_1-\omega_2}(j_1, j_2, \alpha)\Gamma_\alpha|^2. \quad (20)$$

For a two-port resonator we use the input and output coefficient κ_{in} and κ_{out} [11]. In this case the power coupled to the load is

$$P_L = \kappa_{\text{out}} P_d = \kappa_{\text{out}} \frac{(2\omega_1-\omega_2)W_0}{Q_0}|H_{2\omega_1-\omega_2}|^2 \quad (21)$$

and, similarly to Eq. (19), j_1, j_2 can be related to the power available from the sources through

$$\frac{4P_{0,\omega_1}\kappa_{\text{in}}}{(1+\kappa_{\text{in}}+\kappa_{\text{out}})^2} = \frac{\omega_1 W_0}{Q_0}|j_1|^2 \quad (22)$$

and the resulting equation for P_L is

$$P_L = (4P_{0,\omega_1})^\alpha (4P_{0,\omega_2}) \left(\frac{Q_0}{\omega_0 W_0}\right)^{\alpha+2} \frac{\kappa_{\text{out}}\kappa_{\text{in}}^{\alpha+1}}{(1+\kappa_{\text{out}}+\kappa_{\text{in}})^{2(\alpha+2)}} |[\Delta R_\alpha + j(2\omega_1-\omega_2)\Delta L_\alpha] T_{2\omega_1-\omega_2}(j_1, j_2, \alpha)\Gamma_\alpha|^2. \quad (23)$$

Equations (20) and (23) are the general equations that relate the measured intermodulation power with the parameters of the film ΔR_α, ΔL_α, and α. In these equations ΔR_α and ΔL_α only affect the level of the intermodulation products, but not the slope of their variation with the source power. On the other hand, α affects both the IMD level and the slope. This can also be seen from the equations of the intermodulation electric field (Eqs. (4), (6), and (7)), and from those of the intermodulation magnetic field (Eqs. (8) and (16)).

Note that we are assuming that the surface current amplitudes j_1, j_2 in Eq. (16) (or, equivalently, the tangential component of the magnetic fields on the HTS surface H_{ω_1}, H_{ω_2}) are identical to those that would be on the HTS if it was completely linear (see Eqs. (19) and (22)). In other words, we do not take into account the compression effect that occurs at high

power levels, when a significant fraction of the power that is injected to the resonator at ω_1 and ω_2 is transferred to other frequencies ($2\omega_1 - \omega_2$, $2\omega_2 - \omega_1$, and others) by the effect of the nonlinearities, thereby reducing the amplitude of the fields and currents at ω_1 and ω_2.

4. ANALYSIS OF A RUTILE-LOADED CAVITY

In this section we will apply the general analysis described in the preceding one to the dielectric-loaded resonator cavity of Fig. 4. We will analyze a TE_{011} rutile resonator similar to the one described in [12], but the analysis may also be applied to similar resonators with other dielectric materials (like sapphire) which are commonly used in microwave HTS characterization. We have chosen to use a rutile dielectric because it avoids high fringing fields in the normal-metal housing of the resonator, thus limiting the effect of housing loss in the overall Q of the resonator despite the small dimensions of the cavity. The TE_{011} mode used has the advantage of avoiding "wrap around" effects which—as described in [13]—enhance the nonlinearities in the device and make the IMD very strongly dependent on the properties of narrow areas of the HTS film. In these conditions, the current density on the HTS endplate in an intermodulation experiment can be written as

$$\vec{j}s(\rho, t) = (j_1 \cos\omega_1 t + j_2 \cos\omega_2 t)\, f(\rho)\hat{\phi}, \qquad (24)$$

where $\hat{\phi}$ is the unit vector in the azimuth direction and f(ρ) describes the radial dependence of the TE_{011} mode which, according to [14], is

$$f(\rho) = \begin{cases} \dfrac{\beta}{\xi_1} J_1(\xi_1\rho) & \rho \le a \\ \dfrac{\beta}{\xi_2}\dfrac{J_0(\xi_1\rho)}{F_0(\xi_2\rho)} F_1(\xi_2\rho) & b > \rho > a \end{cases}, \qquad (25)$$

where β is the z-direction propagation constant, ξ_1 and ξ_2 are the ρ-direction wave numbers (inside and outside the dielectric, respecti vely), $F_0(\xi_2\rho) = I_0(\xi_2\rho) + K_0(\xi_2\rho)I_1(\xi_2 b)/K_1(\xi_2 b)$, $F_1(\xi_2\rho) = -I_1(\xi_2\rho) + \boldsymbol{K_1(\xi_2\rho)}\mathrm{I_1}\boldsymbol{(\xi_{2b})/K_1(\xi_2\rho)}$ being J_0, I_1, I_2, K_0, K_1 the corresponding Bessel and Hankel functions. From this current distribution and analyzing the cavity as described in the previous section, we obtain

$$\vec{H}_{2\omega_1-\omega_2}(\rho) = [\Delta R_\alpha + j(2\omega_1 - \omega_2)\Delta L_\alpha] T_{2\omega_1-\omega_2} (j_1, j_2, \alpha) j_1^\alpha j_2 \Gamma_\alpha \frac{Q_L}{(2\omega_1 - \omega_2)W_0} f(\rho)\hat{\rho}, \qquad (26)$$

where

$$\Gamma_\alpha = \pi \left[\left| \frac{\beta}{\xi_1} \right|^{\alpha+2} IJ_{2+\alpha} + \left| \frac{\beta}{\xi_2} \frac{J_0(a\xi_1)}{F_0(a\xi_2)} \right|^{\alpha+2} IF_{2+\alpha} \right] \qquad (27)$$

and $IJ_{2+\alpha} = \int_0^\alpha |J_1(\xi_1\rho)|^{2+\alpha}\rho\, d\rho$, $IF_{2+\alpha} = \int_a^b |F_1(\xi_2\rho)|^{2+\alpha}\rho\, d\rho$. The resulting power coupled out the cavity at $2\omega_1 - \omega_2$ is obtained from Eq. (20).

Once we know the $\vec{H}_{2\omega_1-\omega_2}$ generated by one HTS endplate, we can easily extend our study to a cavity having two nonlinear endplates. In this case, the integral in Eq. (14) has to be done over the two HTS endplates. As a result the value of $H_{2\omega_1-\omega_2}$ is the sum of the contribution of each endplate, and can be calculated by applying Eq. (26) to each of them.

5. MEASUREMENTS AND DATA FITTING

Measurements were made with the resonator shown in Fig. 4, which has a 3-mm high rutile rod (4-mm diameter) of $\varepsilon_r \sim 110$ at 77 k, sandwiched between two 10×10 mm^2 endplates. The resonant frequency of the TE_{011} mode is close to 8 GHz.

To make the IMD measurements, the input port is fed with two signals at frequencies f_1 and f_2, both within the passband of the resonator. The power of these sources is either varied simultaneously (balanced measurements), or is changed in only one of the sources, leaving the second tone power constant (unbalanced measurements). Coupling is made by an adjustable coupling loop. The intermodulation products are measured with a one-port setup (see Fig. 5) in which a spectrum analyzer (SA) is used to measure the signals going out of the resonator. The SA is kept isolated from the generators producing the signals at f_1 and f_2 so that, if the resonator is critically coupled, the power of the signals at f_1 and f_2

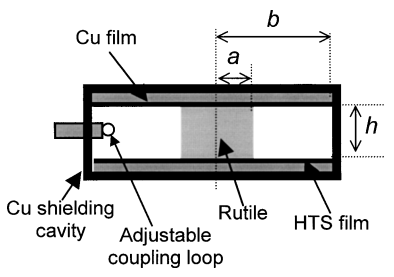

Fig. 4. Dielectric resonator structure used for IMD characterization of HTS films.

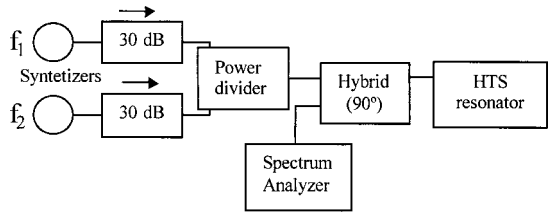

Fig. 5. Block diagram of the one port measurement setup.

reaching the SA is very small, and the IMD of the SA does not alter the measurements of the power of the intermodulation products at $2f_1 - f_2$ and $2f_2 - f_1$. Furthermore, in this arrangement the spectral purity of the sources is not as critical as it is in transmission measurements, where the intermodulation products are easily masked by the phase noise of the sources if $|f_1 - f_2|$ is not sufficiently large.

All the measurements made for characterization were done with the resonator immersed in liquid nitrogen. However, comparative measurements were also made in a closed-cycle cryostat to ensure that thermal effects were not dominant in the generation of intermodulation products. In these measurements, if the power applied to the resonator was sufficiently large, we observed variations of the resonant frequency which we attributed to heating effects on the rutile [12]. This variations were small if the source power was sufficiently low. In these conditions the IMD products measured compared well (within 0.5 dB) with those made in liquid nitrogen immersion.

A second technique to check for thermal effects is to change the frequency of the envelope of the signal coupled into the resonator ($|f_1 - f_2|/2$). We have performed such measurements by changing $|f_1 - f_2|$ between 1 and 40 KHz, and found consistent results (i.e., variations with $|f_1 - f_2|$, within a 0.5 dB).

Four different endplates have been used in these measurements. Three of them (samples HTS_1, HTS_2, and HTS_3) are 700-nm thick Y-Ba_2-Cu_3-$O_{7-\delta}$ (YBCO) films grown on 0.5-mm MgO substrates by a commercial supplier (Theva), and a fourth one made of copper. The HTS films were used as delivered by the supplier, with no further processing on our part. We made a round-robin series of small signal Q measurements using all the HTS endplates to rule out a large spread in R_s among the films. The average R_s at 77 K was 0.3 $m\Omega$ and we can guarantee that the spread is less than 25%, but our capability to assure this is limited by the loss of the rutile, so the real spread in R_s might be lower. Nonlinear measurements where made with the combination of endplates shown in Table I.

Table I. Endplates Used in the Nonlinear Resonator Measurements ($T = 77$ K)

Set	Films	Q_L	Q_0
1	HTS_1–Cu	8000	16000
2	HTS_2–Cu	6500	16000
3	HTS_1–HTS_2	17500	80000
4	HTS_3–Cu	8000	16000
5	HTS_2–HTS_3	16000	77000

Figure 6 shows the results of the IMD measurements of sets 1 and 2, which reveal very strong differences in the intermodulation performance of samples HTS_1 and HTS_2. For example, the intermodulation products obtained from balanced measurements at 0 dBm in set 1 are 20 dB higher than those of set 2, which cannot be justified by the difference in Q_L.

By applying Eq. (20) to set 1 and set 2 and assuming that resistive nonlinearities are negligible [2,4] we have extracted the nonlinear parameters of HTS_1 and HTS_2. The resulting values are $\alpha_1 = 0.2$, $\Delta L_{\alpha 1} = 5 \times 10^{-16}\,\mathrm{Hm}^{0.2}/A^{0.2}$ and $\alpha_2 = 1$, $\Delta L_{\alpha 2} = 3.5 \times 10^{-19}\,\mathrm{Hm}/A$, respectively. Figure 7 shows the resulting $b_{\mathrm{NL}}(j_s)$ for each of the two sets in the range of current densities used in our experiments.

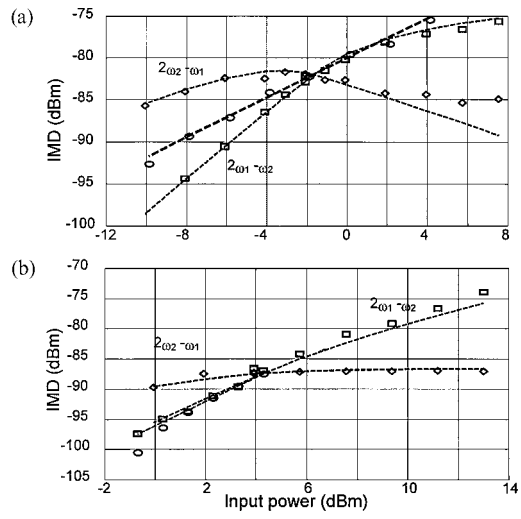

Fig. 6. Results of measurements and fittings (lines) for set 1 (a) and set 2 (b). Circles: measured power of intermodulation products at $2\omega_1 - \omega_2$ as a function of the source power when the power of both sources was increased simultaneously. Squares and diamonds represent the measured power of the intermodulation products at $2\omega_1 - \omega_2$ and $2\omega_2 - \omega_1$, respectively, as a function of the source power at ω_1 when the power of the source at ω_2 was kept constant at −2 dBm in set 1 and 4 dBm in set 2. The difference between the two source frequencies is 20 KHz.

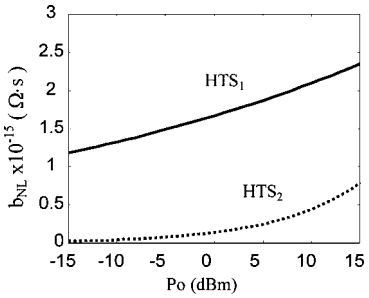

Fig. 7. Plot of $b_{\mathrm{NL}}(j_s)$ for set 1 and set 2 for the range of source power used in the measurements.

Once HTS_1 and HTS_2 are characterized we have extended our experiments to a resonator having both HTS_1 and HTS_2 as endplates (set 3 in Table I). Figure 8 shows the results of the balanced and unbalanced IMD measurements made with this set versus the theoretical results predicted using the values of α and ΔL_α found above, from sets 1 and 2.

The IMD of set 4 (HTS_3 and the Cu endplate) was below the sensitivity of our measurement setup (-95 dBm for an available power of 10 dBm at the resonator port). Coupling in this set was adjusted to obtain the same circulating power than that in set 1 and set 2. This indicates that the HTS nonlinearities of the three samples are very different, and that there is no contribution of the measurement setup to the IMD measurements of sets 1 and 2. Measurable levels of IMD were obtained by combining HTS_3 and HTS_2 in set 5, and we obtained results that are consistent with the other sets (larger IMD than set 2). Characterization of the nonlinearities in sample HTS_3 requires improvements in our measurement setup that we are currently addressing.

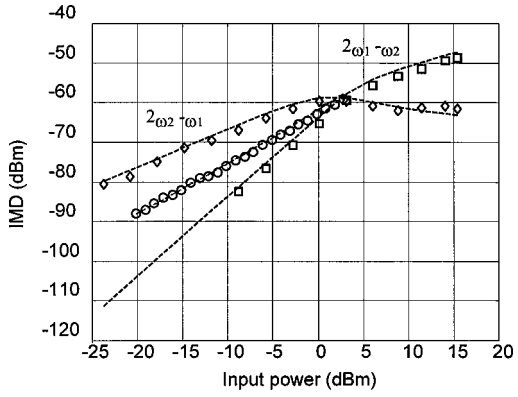

Fig. 8. Results of measurements and calculations for set 3. Circles: measured power of intermodulation products at $2\omega_1 - \omega_2$ as a function of the source power when the power of both sources was increased simultaneously. Squares and diamonds represent the measured power of the intermodulation products at $2\omega_1 - \omega_2$ and $2\omega_2 - \omega_1$, respectively, as a function of the source power at ω_1 when the power of the source at ω_2 was kept constant at 3 dBm. The lines in the figure are results of calculations performed with parameters obtained from set 1 and set 2. The difference between the two source frequencies is 20 KHz.

6. CONCLUSIONS

We have developed a general technique to calculate intermodulation distortion in resonators with HTS materials. We have applied this technique to a rutile resonator to use it for characterization of the nonlinear properties of unpatterned 10×10 mm^2 HTS films. We have found that three state-of-the-art HTS samples can have widely different IMD performance, while having a moderate spread in R_s. We encourage other groups to try this technique so that data can be accumulated for a larger number of HTS samples, and offer our collaboration to supply further details on the resonator and measurement setup.

Possible improvements in this technique are related to the possibility of extending the validity of the mathematical formulation used for the HTS nonlinearities to fit the wide range of experimental results found in the literature. The formulation in this work is based on the assumption that the same power law can be applied for the resistive and reactive nonlinearities. While this is a severe restriction, it allows to use our technique in the numerous works that claim that, at low powers, the intermodulation products in HTS devices are due to a current dependence of the penetration depth, since this makes the reactive nonlinearities dominant [7,8].

We also note that, while it may be possible to extend the mathematical formulation in this work to consider nonlinear functions other than the power law ($a_{\mathrm{NL}}(j_s) = \Delta R_\alpha |J_s|^\alpha$, $b_{\mathrm{NL}}(j_s) = \Delta L_\alpha |j_s|^\alpha$), and allow different types of nonlinear functions in the resistive and reactive nonlinearities ($a_{\mathrm{NL}}(j_s)$ and $b_{\mathrm{NL}}(j_s)$), these extended abilities can already be achieved with numerical calculations as described in [15].

ACKNOWLEDGMENTS

This work has been funded by Spanish Ministry of Education and Culture through Project No. MAT2002–04551–C03–03 and Scholarship AP99

78085980, and by the Generalitat de Catalunya through Scholarship 2002 FI 00622.

REFERENCES

1. B. A. Willemsen, T. Dahm, B. H. King, and D. J. Scalapino, *IEEE Trans. Appl. Supercond.* **9**(4), 4181 (1991).
2. B. A. Willemsen, T. Dahm, and D. J. Scalapino, *Appl. Phys. Lett.* **71**(29), 3898 (1997).
3. D. Oates, A. Anderson, D. Sheen, and S. Ali, *IEEE Trans. Microwave Theory Tech.* **39**(9), 1522 (1991).
4. J. Booth, J. Bell, D. Rudman, L. Vale, and R. Ono, *J. Appl. Phys.* **86**(2), 1020 (1999).
5. J. Mateu, C. Collado, and J. O'Callaghan, *IEEE Trans. Appl. Supercond.* **11**(1), 135–138 (2001).
6. J. Parrón, C. Collado, J. Mateu, J. Rius, N. Duffo, and J. O'Callaghan, *IEEE Trans. Appl. Supercond.* **11**(1), 399–402 (2001).
7. T. Dahm and D. Scalapino, *J. Appl. Phys.* **81**(4), 2002 (1997).
8. R. Hammond, E. Soares, B. Willemsen, T. Dahm, D. Scalapino, and J. Schrieffer, *J. Appl. Phys.* **84**(10), 5662 (1998).
9. C. Collado, J. Mateu, T. Shaw, and J. O'Callaghan, *Physica C* **372–376**(P1), 566–570 (2002).
10. B. Willemsen, K. Kihlstrom, and T. Dahm, *Appl. Phys. Lett.* **74**(5), 753 (1999).
11. M. J. Lancaster, *Passive Microwave Device Applications of High-Temperature Superconductors* (Cambridge University Press, Cambridge, England, 1997).
12. N. Klein, C. Zuccaro, U. Dähne, H. Schulz, and N. Tellmann, *J. Appl. Phys.* **78**(11), 6683–6686 (1995).
13. Z. Y. Shen, C. Wilker, P. Pang, D. W. Face, C. F. C. III, and C. M. Harrington, *IEEE Trans. Appl. Supercond.* **7**(2), 2446–2453 (1997).
14. J. Mazierska and R. Grabovickic, *IEEE Trans. Appl. Supercond.* **8**(4), 178–187 (1998).
15. J. Mateu, C. Collado, T. J. Shaw, and J. O'Callaghan, *Physica C* **372–376**(P2), 679–682 (2002).